

Non-Boltzmann thermoelectric transport in minimally twisted bilayer graphene

Bhaskar Ghawri,^{1,*} Phanibhusan S. Mahapatra^{1,†}, Manjari Garg,^{2,‡} Shinjan Mandal,¹ Aditya Jayaraman,¹ Kenji Watanabe³, Takashi Taniguchi,⁴ Manish Jain,¹ U. Chandni,² and Arindam Ghosh^{1,5,§}

¹*Department of Physics, Indian Institute of Science, Bangalore 560012, India*

²*Department of Instrumentation and Applied Physics, Indian Institute of Science, Bangalore 560012, India*

³*Research Center for Functional Materials, National Institute for Materials Science, Namiki 1-1, Tsukuba, Ibaraki 305-0044, Japan*

⁴*International Center for Materials Nanoarchitectonics, National Institute for Materials Science, Namiki 1-1, Tsukuba, Ibaraki 305-0044, Japan*

⁵*Centre for Nano Science and Engineering, Indian Institute of Science, Bangalore 560 012, India*



(Received 21 January 2023; revised 13 December 2023; accepted 20 December 2023; published 30 January 2024)

The electronic bands formed in moiré systems with twisted bilayer graphene (tBLG) have emerged as a tunable platform for studying many novel concepts of condensed matter physics due to new interaction and topological effects. In particular, the multitude of closely packed flat bands and a sequence of van Hove singularities (vHSs) in minimally tBLG can not only lead to nontrivial topological transport but also the breakdown of conventional Boltzmann transport formalism due to the competition between the scales of energy variation within the system and that of the external parameters such as temperature or electric field. Here, we demonstrate the violation of the semiclassical Mott relation in small-angle tBLG ($\theta \sim 0.45^\circ$) even at room temperature, which we associate to a narrow diverging density of states. We also show the emergence of nonlinear effects in thermovoltage by exploiting vertical thermoelectric transport in an atomically thin tBLG device. Our results not only point towards the fundamental limitations of the applicability of the semiclassical Boltzmann approach in small-angle tBLG but also outline an experimental approach that can lead to the discovery of different broken-symmetry states.

DOI: [10.1103/PhysRevB.109.045436](https://doi.org/10.1103/PhysRevB.109.045436)

I. INTRODUCTION

The semiclassical Boltzmann transport approach (BTA) and relaxation time approximation are central to the understanding of transport properties in most conventional metals and semiconductors [1]. Within this framework, the transport properties can be described by assuming that the density of states (DOS) near the Fermi energy (E_F) varies slowly on the scale of thermal energy ($k_B T$), where only a fixed population of electrons within the energy range of a few $k_B T$ around E_F contribute to both charge and heat transport. However, when the DOS changes rapidly with energy at E_F , changes in temperature can modify the effective number of charge carriers and the scattering probability. This effect, commonly known as Mott-Fermi thermal smearing of energy levels, can lead to distinctive transport properties [2–5]. In addition, the divergent DOS at van Hove singularities (vHSs), in many cases, drives the onset of correlated electronic phases, such as superconductivity [6], magnetism [7,8], and density waves [9,10]. Owing to the presence of a multitude of closely packed flat bands and a sequence of vHSs [11,12], the minimally twisted bilayer graphene (tBLG) not only provides an ideal platform to test the validity of semiclassical BTA but the many-body phases that can arise due to diverging DOS

can also be explored. However, it requires a measurement technique that is extremely sensitive to the variation of the DOS.

In this paper, we have performed electrical and thermoelectric measurements in small-angle tBLG ($\theta \sim 0.45^\circ$), both in in-plane and vertical device geometry. We use the dependence of thermal voltage on the carrier density (n), T , and temperature gradient (ΔT) as a sensitive probe for the low-energy features in the band structure. In degenerate metals and semiconductors ($T \ll T_F$, where T_F is the Fermi temperature), the electric and thermoelectric transport coefficients can be related through the Mott relation (MR), obtained within the semiclassical Boltzmann framework

$$S_{\text{Mott}} = \frac{\pi^2 k_B^2 T}{3|e|} \left. \frac{d \ln R(E)}{dE} \right|_{E_F}, \quad (1)$$

where R and e are the resistance and electronic charge, respectively. MR effectively arises from the assumption that the thermal energy of the conduction electrons is much smaller than the scale of any structure in the electronic DOS near the Fermi energy. Although the validity of the MR has been verified experimentally for many decades in various materials, such as metals/semiconductors [13,14], graphene [15,16], and topological insulators [17], it can be violated due to Mott-Fermi smearing in systems having sharp features in DOS such as transition and rare earth metals [2,3,18]. Thus, the validity of MR provides a sensitive probe to the energy distribution of the charge carriers near the Fermi surface. Furthermore, the thermal response of the system also allows us to probe the

*gbhaskar@iisc.ac.in

†phanis@iisc.ac.in

‡manjarigarg@iisc.ac.in

§arindam@iisc.ac.in

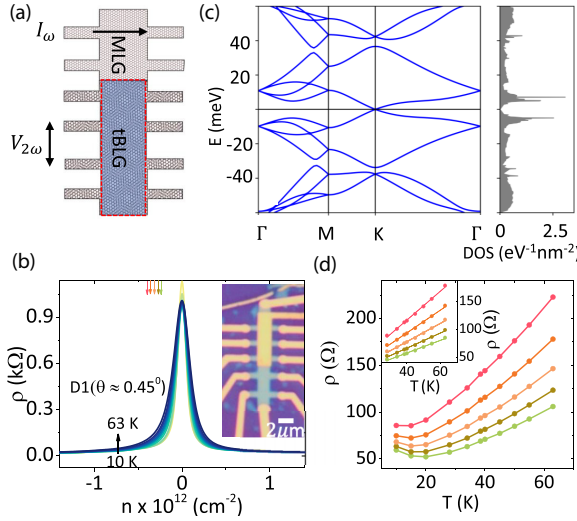


FIG. 1. Device structure and electrical transport in device D1. (a) Schematic of a type-1 device (in-plane geometry), showing the tBLG channel, monolayer part (heater), and the top gate (dotted red rectangle). (b) ρ as a function of n at various temperatures. The inset shows the optical micrograph of the device. (c) Electronic band structure and density of states (DOS) of tBLG (0.5°) calculated using tight-binding model. (d) ρ as a function of T at a few selected densities [marked by arrows in (b)]. The inset shows the linear fits to the data in the metallic regime.

nonlinear effects that can arise due to the divergent DOS and electronic correlations [19–22].

II. RESULTS AND DISCUSSION

The tBLG devices in this study consist of two graphene layers stacked at θ [in-plane geometry, type 1, Fig. 1(a)] or $\theta + 60$ [vertical geometry, type 2, Fig. 3(a)], where θ is the twist angle. We study three different devices with $\theta \approx 0.45^\circ$ (D1), $\theta \sim 5^\circ$ (D3) fabricated in type-1 geometry, and $\theta \approx 0.43^\circ$ (D2) in type-2 geometry. We have used Raman spectroscopy to estimate the twist angle for device D3 [see Supplemental Material (SM) [23]], whereas thermoelectric (electrical and thermoelectric) transport is used to calculate the twist angle for device D1 (D2). A type-1 device is etched into a standard Hall bar geometry and consists of both monolayer graphene (MLG) and tBLG regions. A local top gate is used to tune the n in the overlap region [inset of Fig. 1(b)]. The MLG channel outside the top-gated region is used as a heater to set up a ΔT across the tBLG channel for thermoelectric measurements. The details on the type-2 device are presented later.

We first focus on transport in the in-plane direction (device D1). Figure 1(b) shows the density-dependent resistivity ρ measured at various temperatures. We observe resistance maxima only at the charge neutrality point (CNP) with no sign of resistive feature corresponding to the vHSs or full filling ($\nu = \pm 4$) of the lowest bands. The observed behavior is in agreement with the tight-binding calculation for the electronic band structure, which shows the absence of a band gap between the first and second moiré bands and renders it hard to observe any feature in the range of T investigated

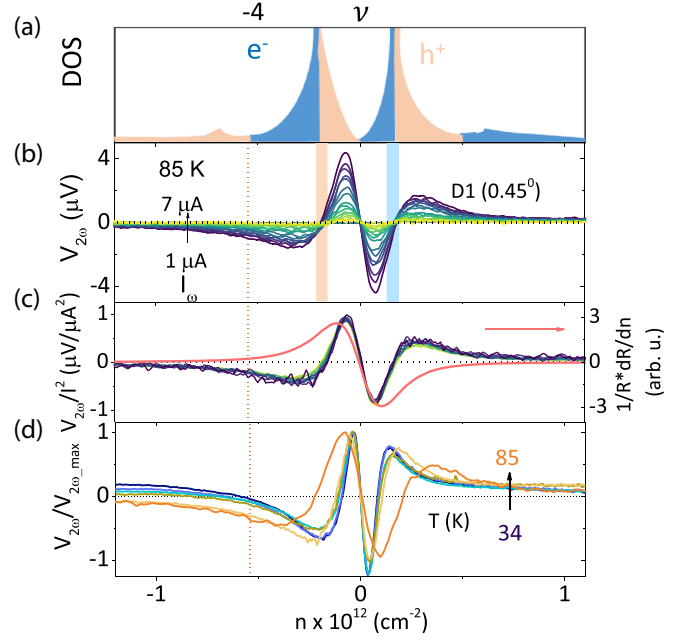


FIG. 2. Thermoelectric transport in device D1: (a) Schematic showing the variation of DOS as a function of n . (b) $V_{2\omega}$ as a function of n for different I_ω at 85 K. The shaded bars indicate the observed Lifshitz transitions. (c) $V_{2\omega}$ normalized with I_ω^2 . The right axis shows $(1/R)dR/dn$ for comparison. (d) $V_{2\omega}/V_{2\omega,\max}$ as a function of n measured at six different temperatures. The dotted line indicates the zero crossing in thermopower at $\nu = -4$.

[Fig. 1(c)]. The T dependence of ρ shows a clear metallic behavior down to 30 K, except in the immediate vicinity of the CNP [Fig. 1(d)]. The ρ starts to saturate around 20 K, followed by a slight increase as the sample is cooled to 10 K. We believe that the slight increase in ρ could be due to the weak localization (WL) effect, leading to an enhancement of resistivity as the T decreases. However, there are insufficient data points at low temperatures to make any quantitative estimation about WL effects.

To get further insights into the electronic structure, we have performed thermoelectric measurements in the same device. A sinusoidal current (I_ω) is passed through the MLG region, which sets up a ΔT across the tBLG. The resulting second-harmonic thermovoltage ($V_{2\omega}$) is measured across the tBLG region as a function of n and I_ω [15,24]. ΔT was not measured for this device, and only qualitative features in $V_{2\omega}$ are discussed.

$V_{2\omega}$ exhibits multiple sign reversals as E_F is tuned to either side of the CNP at 85 K [Fig. 2(b)]. While the sign reversal near the CNP is due to the change in quasiparticle excitations, those near $n = \pm 0.18 \times 10^{12} \text{ cm}^{-2}$ are a manifestation of a topological Lifshitz transition, which represents a transition from a holelike (electronlike) system to an electronlike (holelike) system when E_F is tuned across the vHSs, as shown schematically in Fig. 2(a) [25,26].

Figure 2(c) shows a uniform current scaling of $V_{2\omega}$, thereby ensuring the thermal origin. Additionally, for hole doping as the E_F is tuned into the next band, we observe a weak sign inversion in $V_{2\omega}$ as T is reduced below 45 K [dotted line in Fig. 2(d)], which corresponds to the $\nu = -4$ and

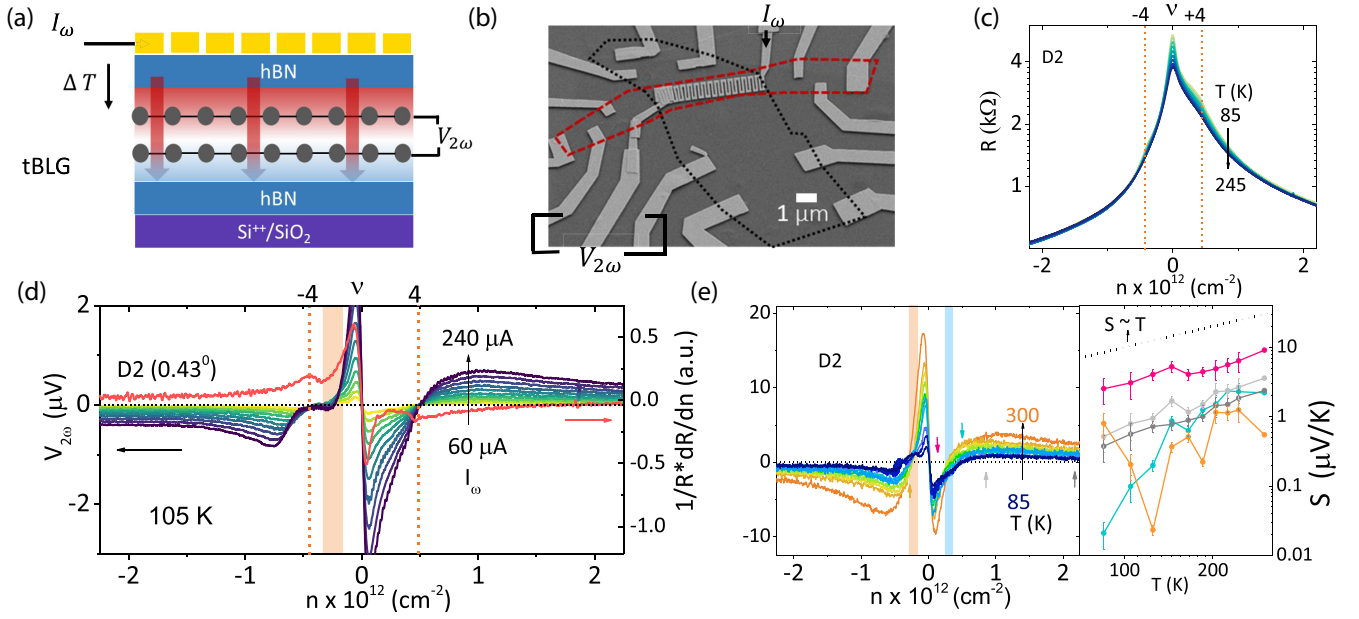


FIG. 3. Vertical transport in device D2: (a) The cross-sectional view of a type-2 device. (b) Scanning microscope image of the device. (c) Resistance as a function of n at various temperatures ranging from 85 to 245 K. (d) $V_{2\omega}$ as a function of n for different values of I_{ω} at 105 K. The shaded bar indicates the Lifshitz transition on the hole doping and the dotted lines show the position of $\nu = \pm 4$. The right axis shows $(1/R)dR/dn$ for comparison. (e) S as a function of n at different temperatures. The right panel shows the T dependence of S at various band fillings marked with arrows. The black line shows the linear- T dependence as a guide for eye.

thus allows us to calculate the angle. Notably, we do not find any feature associated with $\nu = +4$, clearly indicating particle-hole asymmetry. Remarkably, no corresponding features were observed in resistance at $\nu = \pm 4$, as discussed already in Fig. 1(b), which indicates the extreme sensitivity of thermopower to the fine details of the band structure.

Next, in order to connect resistance and thermopower, we employ MR and rewrite Eq. (1) as

$$S_{\text{Mott}} = \frac{\pi^2 k_B^2 T}{3|e|} \frac{1}{R} \frac{dR}{dV_{\text{tg}}} \frac{dV_{\text{tg}}}{dn} \frac{dn}{dE} \Big|_{E_F}, \quad (2)$$

where $(1/R)dR/dV_{\text{tg}}$ is measured experimentally and determines the sign of the Mott thermopower. dn/dE is the DOS. ($dV_{\text{tg}}/dn = e/C_{\text{hBN}}$, where C_{hBN} is the top-gate capacitance per unit area.) The difficulty in accurately estimating the DOS for low-angle tBLG prohibits us from accurately calculating the S_{Mott} and we focus on the qualitative comparison between the measured $V_{2\omega}$ and $\alpha = (1/R)dR/dn$. We find that α qualitatively captures the thermopower behavior near the CNP, but fails to predict the sign reversal in $V_{2\omega}$ at the Lifshitz transition and hence leads to an apparent violation of the MR [Fig. 2(c)]. For reference, we present the results from device D3 in Sec. IA in the Supplemental Material [23]. We find that $V_{2\omega}$ matches qualitatively with S_{Mott} over the experimental range of n , thereby confirming the validity of MR at large angles.

In order to confirm the generality of the correlation between transport and the unique band structure in minimally tBLG, we have complemented the in-plane measurements with electrical and thermoelectric probing in the out-of-plane vertical geometry [Fig. 3(a)]. Device D2 consists of a cross junction of two graphene layers with a microfabricated heater on the top of the twisted region [Fig. 3(b)], which is used

to create a ΔT perpendicular to the plane of tBLG and the resultant $V_{2\omega}$ is measured across two graphene layers. We find that, unlike device D1, device D2 shows broad peaks on either side of the CNP [Fig. 3(c)], which we identify as $\nu = \pm 4$ (as verified by thermoelectric measurements shown later). The peaks at the CNP show an insulating behavior throughout the measured T range, whereas shoulder peaks at $\nu = \pm 4$ show weak insulating behavior and start vanishing above $T \sim 145$ K.

Similar to device D1, we observe a Lifshitz transition as well as the breakdown of MR on either side of the CNP [Fig. 3(d)]. In addition, for hole doping, as the E_F is tuned into the next band, we observe a weak sign inversion in $V_{2\omega}$ [dotted line in Fig. 3(d)], which corresponds to $\nu = -4$. In contrast, for the electron side, thermal broadening leads to a single sign reversal (light-blue-shaded region). Using the ΔT calculated from the resistance thermometry (for additional details, see Supplemental Material [23]), we plot the n dependence of $S = V_{2\omega}/\Delta T$ for different temperatures [left panel, Fig. 3(e)]. We observe that the sign inversion at the Lifshitz transition persists up to 300 K, whereas thermal broadening smears the sign inversion at $\nu = -4$ at $T \geq 145$ K. The observation of weak resistive peaks at $\nu = \pm 4$, Lifshitz transitions, and sign reversal at $\nu = -4$ in thermopower, even at elevated T , suggests that the vertical transport is more sensitive to the band structure than the in-plane transport, presumably due to reduced disorder (and angle inhomogeneity)-induced broadening as the effective “length” of the sample is significantly smaller in the vertical geometry. Further, S exhibits a linear dependence on T at all dopings except in the vicinity of vHSS [right panel, Fig. 3(e)]. The $S \propto T$ behavior is expected in semimetals and metals within the semiclassical framework and has been verified for MLG [15] as well as tBLG at larger

θ ($2^\circ \lesssim \theta \lesssim 5^\circ$) [27]. Close to vHSs, however, we find an unusual nonmonotonic T dependence of S , which points towards a departure from the semiclassical approach. We want to note that, although the observed sign reversal at vHSs and full filling of the band can also be observed within the semiclassical Boltzmann formalism, the temperature scales do not match at all (see Fig. S6 in the Supplemental Material [23], and see also Refs. [28–31] for calculation details).

The sign reversal in $V_{2\omega}$ at the Lifshitz transition and nonmonotonic T dependence of S in the vicinity of vHSs indicate the breakdown of the MR. Although the MR has been verified in a range of graphene-based devices [15,16], recent reports suggest an emergent breakdown of this formalism near/at the magic angle [32,33] and in marginally tBLG [34], though at lower temperatures ($T < 40$ K) when strong correlation effects become important. The observed discrepancy from the MR can be discussed by scrutinizing the assumptions made in deriving Eq. (2). First, it relies on the Sommerfeld approximation, which in principle should be valid for $T \ll T_F$. Theoretical calculations suggest a bandwidth of ~ 10 – 12 meV [Fig. 1(c)], leading to $T_F \sim 100$ K, which satisfies the condition $T \ll T_F$ for the lowest temperature (~ 30 K) used in the experiments. Further, as discussed earlier, MR assumes that the electronic spectrum near E_F does not vary appreciably on the thermal energy scale. However, theoretical calculations suggest that DOS near vHSs vary sharply on the scale of ~ 1 meV [right panel, Fig. 1(c)] and can lead to the smearing of the Fermi function in the vicinity of the Fermi energy and higher-order temperature-dependent corrections in thermopower cannot be neglected. This smearing of the Fermi function is likely to lead to a Mott violation in small-angle tBLG. Another intriguing possibility is the appearance of non-Fermi-liquid (NFL) behavior in the presence of the vHS [35,36]. The key signature of the NFL is logarithmically diverging S/T at low T . Although our data suggest a nonmonotonic temperature dependence of S near the vHSs, there is not enough experimental resolution at this point to investigate S/T behavior quantitatively and requires further experiments in a wide range of T .

We finally focus on the anomalous dependence of $V_{2\omega}$ on I_ω in device D2 in the hole-doped regime. We plot $V_{2\omega}$ normalized with I_ω^2 in Fig. 4(a), which shows a uniform scaling except in the density range near vHS and $\nu = -4$ (sky-blue-shaded region). Interestingly, the nonlinearity onsets at 85 K, becomes prominent at 105 and 125 K, and nearly vanishes when the temperature is increased above 145 K. The nonlinear thermoelectric response only in a specific n and T range is intriguing and suggests a departure from the conventional semiclassical description. The nonlinearity, in general, can arise due to ΔT -induced renormalization effects, resulting in a transmission function $\Gamma(E, \Delta T)$ [37–39] or due to the variation of $\Gamma(E)$ with E on the energy scale $k_B \Delta T$ [38]. However, the appearance of nonlinearity only in a narrow intermediate T range rules out the above two scenarios. Further, the position of sign reversal at $\nu = -4$ shifts gradually to higher hole doping as I_ω is increased, whereas the position of vHS first shifts to lower n and then moves to higher doping as shown in Figs. 4(b) and 4(c). We characterize the effective shift in sign reversals by calculating Δn [Fig. 4(c)], which gives the

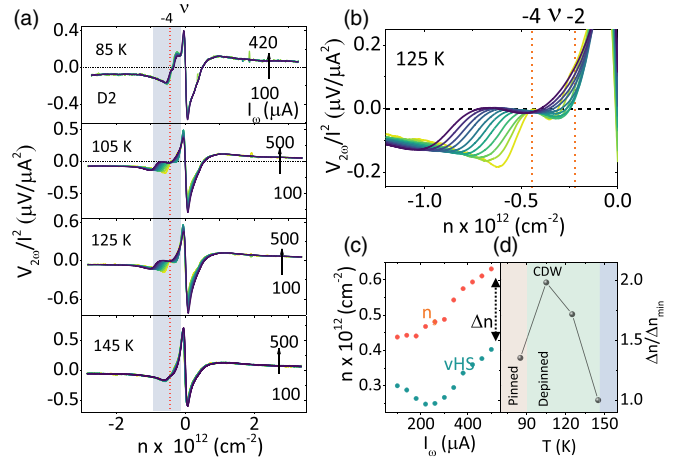


FIG. 4. Nonlinear thermoelectric transport in device D2: (a) $V_{2\omega}$ normalized with I_ω^2 as a function of n at four different temperatures. $V_{2\omega}$ shows a uniform current scaling except in the density range near vHS and $\nu = -4$ (sky-blue-shaded region) in the intermediate T range and vanishes as the temperature is increased to 145 K. (b) $V_{2\omega}/I_\omega^2$ zoomed in near vHS and $\nu = -4$, showing the shift in the position of sign reversal at vHS and $\nu = -4$ as the heating current is increased. (c) Shift in the position of vHS and $\nu = -4$ as a function of I_ω , where Δn defines the difference between the position of vHS and $\nu = -4$ at maximum I_ω . (d) Variation of $\Delta n/\Delta n_{\min}$ as a function of T , where Δn_{\min} corresponds to difference in position of vHS and $\nu = -4$ at 145 K. Shaded regions indicate the possible pinned and depinned charge density wave (CDW) phases.

difference in the position of vHS and $\nu = -4$ at maximum current (~ 500 μA). The magnitude of Δn becomes maximum at 105 K and approaches the low current value (difference in the position of vHS and $\nu = -4$ at 100 μA) as the T is raised to 145 K [Fig. 4(d)]. The observed shift in the density corresponding to vHS and $\nu = -4$ indicates the malleability of the low-energy bands, which, although not uncommon in tBLG, has been observed only with respect to the tuning of E_F across the lowest-energy bands [40,41]. Previous experiments in magic-angle tBLG have revealed broken-symmetry states at half-integer band fillings, which could arise from a spin or charge density wave (CDW) ground state at zero magnetic field [41]. We speculate that the nonlinear response can also arise from the depinning of an underlying phase associated with CDW formation, as seen previously in electrical transport in NbSe_3 [22,42,43] and other one-dimensional organic conductors [44,45]. Our findings suggest that the application of a thermal stimulus leads to the depinning of the CDW, similar to the depinning of CDW by the electric field in NbSe_3 [22] and other systems [44,46]. However, the nature of the CDW phase (if any) in our experiments is not very clear at this point, and more experiments involving frequency-dependent transport measurements, along with theoretical studies, are required for a better understanding. Alternatively, entropy-driven phase transitions, in which the system develops finite isospin polarization even at high temperatures (~ 4 – 80 K) [47–49], can also lead to observed shifts in sign reversals and nonlinear thermopower, but a complete understanding requires further studies.

III. CONCLUSION

In summary, we have measured the resistivity and thermopower in small-angle tBLG in two different geometries. We have demonstrated the extreme sensitivity of thermopower to low-energy features in tBLG, with clear signatures of a Lifshitz transition persisting up to room temperature. At $\theta \sim 0.45^\circ$, irrespective of device geometry, our experimental results show a breakdown of the semiclassical MR near vHSs, which is attributed to the Mott-Fermi smearing due to the presence of sharp features in the DOS. In addition, we also show a nonlinear thermoelectric response in vertical transport, which appears to arise due to a new symmetry-broken phase,

but requires further understanding. Our results point towards the fundamental shortcomings of the applicability of the semiclassical Boltzmann approach in such systems.

ACKNOWLEDGMENTS

The authors thank Prof. T. Das and Dr. S. Ray for helpful discussions. The authors acknowledge financial support from Nano mission, DST. K.W. and T.T. acknowledge support from the JSPS KAKENHI (Grants No. 19H05790, No. 20H00354, and No. 21H05233). U.C. acknowledges funding from IISc and SERB (ECR/2017/001566).

B.G., P.S.M., and M.G. contributed equally to this work.

-
- [1] N. W. Ashcroft and N. D. Mermin, *Solid State Physics* (Cengage Learning, Boston, 2022).
- [2] N. F. Mott, *Proc. R. Soc. London A* **153**, 699 (1936).
- [3] N. F. Mott, *Proc. R. Soc. London A* **156**, 368 (1936).
- [4] N. Mott and H. Jones, *The Theory of the Properties of Metals and Alloys* (Oxford University Press, London, 1936).
- [5] A. H. Wilson, *Proc. R. Soc. London A* **167**, 580 (1938).
- [6] X. Shi, Z.-Q. Han, X.-L. Peng, P. Richard, T. Qian, X.-X. Wu, M.-W. Qiu, S. C. Wang, J. P. Hu, Y.-J. Sun, and H. Ding, *Nat. Commun.* **8**, 14988 (2017).
- [7] K. G. Sandeman, G. G. Lonzarich, and A. J. Schofield, *Phys. Rev. Lett.* **90**, 167005 (2003).
- [8] A. Ziletti, S. M. Huang, D. F. Coker, and H. Lin, *Phys. Rev. B* **92**, 085423 (2015).
- [9] H. Isobe, N. F. Q. Yuan, and L. Fu, *Phys. Rev. X* **8**, 041041 (2018).
- [10] V. Kozii, H. Isobe, J. W. F. Venderbos, and L. Fu, *Phys. Rev. B* **99**, 144507 (2019).
- [11] N. N. T. Nam and M. Koshino, *Phys. Rev. B* **96**, 075311 (2017).
- [12] X. Lu, B. Lian, G. Chaudhary, B. A. Piot, G. Romagnoli, K. Watanabe, T. Taniguchi, M. Poggio, A. H. MacDonald, B. A. Bernevig *et al.*, *Proc. Natl. Acad. Sci. USA* **118**, e210006118 (2021).
- [13] D. M. Rowe, *Materials, Preparation, and Characterization in Thermoelectrics* (CRC Press, Boca Raton, FL, 2017).
- [14] K. Behnia, *Fundamentals of Thermoelectricity* (Oxford University Press, Oxford, UK, 2015).
- [15] Y. M. Zuev, W. Chang, and P. Kim, *Phys. Rev. Lett.* **102**, 096807 (2009).
- [16] A. Jayaraman, K. Hsieh, B. Ghawri, P. S. Mahapatra, K. Watanabe, T. Taniguchi, and A. Ghosh, *Nano Lett.* **21**, 1221 (2021).
- [17] D. Kim, P. Syers, N. P. Butch, J. Paglione, and M. S. Fuhrer, *Nano Lett.* **14**, 1701 (2014).
- [18] A. Burkov, D. Kolgunov, K. Hoag, and J. Van Zytveld, *J. Non-Cryst. Solids* **205-207**, 332 (1996).
- [19] S. Datta, *Electronic Transport in Mesoscopic Systems* (Cambridge University Press, Cambridge, UK, 1997).
- [20] H. Linke, W. Sheng, A. Löfgren, H. Xu, P. Omling, and P. Lindelof, *Europhys. Lett.* **44**, 341 (1998).
- [21] T. Christen and M. Büttiker, *Europhys. Lett.* **35**, 523 (1996).
- [22] P. Monceau, J. Richard, and M. Renard, *Phys. Rev. B* **25**, 931 (1982).
- [23] See Supplemental Material at <http://link.aps.org/supplemental/10.1103/PhysRevB.109.045436> for the details on device fabrication and additional transport measurements; twist angle calculation; thermometry used for temperature calibration; and theoretical calculation of the Seebeck coefficient using semiclassical Boltzmann formalism.
- [24] P. S. Mahapatra, K. Sarkar, H. R. Krishnamurthy, S. Mukerjee, and A. Ghosh, *Nano Lett.* **17**, 6822 (2017).
- [25] Y. Kim, P. Herlinger, P. Moon, M. Koshino, T. Taniguchi, K. Watanabe, and J. H. Smet, *Nano Lett.* **16**, 5053 (2016).
- [26] Y. Cao, J. Y. Luo, V. Fatemi, S. Fang, J. D. Sanchez-Yamagishi, K. Watanabe, T. Taniguchi, E. Kaxiras, and P. Jarillo-Herrero, *Phys. Rev. Lett.* **117**, 116804 (2016).
- [27] P. S. Mahapatra, B. Ghawri, M. Garg, S. Mandal, K. Watanabe, T. Taniguchi, M. Jain, S. Mukerjee, and A. Ghosh, *Phys. Rev. Lett.* **125**, 226802 (2020).
- [28] S. Naik, M. H. Naik, I. Maity, and M. Jain, *Comput. Phys. Commun.* **271**, 108184 (2022).
- [29] M. Wen, S. Carr, S. Fang, E. Kaxiras, and E. B. Tadmor, *Phys. Rev. B* **98**, 235404 (2018).
- [30] L. Lindsay and D. A. Broido, *Phys. Rev. B* **81**, 205441 (2010).
- [31] P. Moon and M. Koshino, *Phys. Rev. B* **87**, 205404 (2013).
- [32] B. Ghawri, P. S. Mahapatra, M. Garg, S. Mandal, S. Bhowmik, A. Jayaraman, R. Soni, K. Watanabe, T. Taniguchi, H. Krishnamurthy *et al.*, *Nat. Commun.* **13**, 1522 (2022).
- [33] A. K. Paul, A. Ghosh, S. Chakraborty, U. Roy, R. Dutta, K. Watanabe, T. Taniguchi, A. Panda, A. Agarwala, S. Mukerjee *et al.*, *Nat. Phys.* **18**, 691 (2022).
- [34] P. S. Mahapatra, M. Garg, B. Ghawri, A. Jayaraman, K. Watanabe, T. Taniguchi, A. Ghosh, and U. Chandni, *Nano Lett.* **22**, 5708 (2022).
- [35] J. M. Buhmann and M. Sigrist, *Phys. Rev. B* **88**, 115128 (2013).
- [36] F. Herman, J. Buhmann, M. H. Fischer, and M. Sigrist, *Phys. Rev. B* **99**, 184107 (2019).
- [37] D. Sánchez and R. López, *Phys. Rev. Lett.* **110**, 026804 (2013).
- [38] S. F. Svensson, E. A. Hoffmann, N. Nakpathomkun, P. M. Wu, H. Xu, H. A. Nilsson, D. Sánchez, V. Kashcheyevs, and H. Linke, *New J. Phys.* **15**, 105011 (2013).
- [39] J. Meair and P. Jacquod, *J. Phys.: Condens. Matter* **25**, 082201 (2013).
- [40] S. Wu, Z. Zhang, K. Watanabe, T. Taniguchi, and E. Y. Andrei, *Nat. Mater.* **20**, 488 (2021).
- [41] S. Bhowmik, B. Ghawri, N. Leconte, S. Appalakondaiah, M. Pandey, P. S. Mahapatra, D. Lee, K. Watanabe, T. Taniguchi, J. Jung *et al.*, *Nat. Phys.* **18**, 639 (2022).
- [42] N. P. Ong and P. Monceau, *Phys. Rev. B* **16**, 3443 (1977).
- [43] P. Monceau, *Physica B+C* **109-110**, 1890 (1982).

- [44] M. J. Cohen and A. J. Heeger, [Phys. Rev. B](#) **16**, 688 (1977).
- [45] E. Lopes, M. Matos, R. Henriques, M. Almeida, and J. Dumas, [Europhys. Lett.](#) **27**, 241 (1994).
- [46] Z. Z. Wang, M. Saint-Lager, P. Monceau, M. Renard, P. Gressier, A. Meerschaut, L. Guemas, and J. Rouxel, [Solid State Commun.](#) **46**, 325 (1983).
- [47] Y. Saito, F. Yang, J. Ge, X. Liu, T. Taniguchi, K. Watanabe, J. Li, E. Berg, and A. F. Young, [Nature \(London\)](#) **592**, 220 (2021).
- [48] A. Rozen, J. M. Park, U. Zondiner, Y. Cao, D. Rodan-Legrain, T. Taniguchi, K. Watanabe, Y. Oreg, A. Stern, E. Berg *et al.*, [Nature \(London\)](#) **592**, 214 (2021).
- [49] F. Wu and S. D. Sarma, [Phys. Rev. Lett.](#) **124**, 046403 (2020).